



HAL
open science

In-situ multi-axial testing of three-dimensional (3D) woven organic matrix composites for aeroengine applications

Federico Foti, Yannick Pannier, Salvador Orenes Balaciart, Jean-Claude Grandidier, Marco Gigliotti, Camille Guigon

► **To cite this version:**

Federico Foti, Yannick Pannier, Salvador Orenes Balaciart, Jean-Claude Grandidier, Marco Gigliotti, et al.. In-situ multi-axial testing of three-dimensional (3D) woven organic matrix composites for aeroengine applications. *Composite Structures*, 2021, 273, pp.114259. 10.1016/j.compstruct.2021.114259 . hal-03681353

HAL Id: hal-03681353

<https://hal.science/hal-03681353>

Submitted on 2 Aug 2023

HAL is a multi-disciplinary open access archive for the deposit and dissemination of scientific research documents, whether they are published or not. The documents may come from teaching and research institutions in France or abroad, or from public or private research centers.

L'archive ouverte pluridisciplinaire **HAL**, est destinée au dépôt et à la diffusion de documents scientifiques de niveau recherche, publiés ou non, émanant des établissements d'enseignement et de recherche français ou étrangers, des laboratoires publics ou privés.



Distributed under a Creative Commons Attribution - NonCommercial 4.0 International License

In-situ Multi-Axial Testing of Three-Dimensional (3D) Woven Organic Matrix Composites for AeroEngine Applications

Federico Foti^a, Yannick Pannier^a, Salvador Orenes Balaciart^a, Jean-Claude Grandidier^a, Marco Gigliotti^a

Camille Guigon^b

^aInstitut Pprime, CNRS, ISAE-ENSMA (Department of Physics and Mechanics of Materials),
Université de Poitiers

1, Avenue Clément Ader F-86962 Futuroscope Chasseneuil, France

^bSAFRAN Composites, Conception & Development Department

33, Avenue de la Gare F-91760 Itteville, France

marco.gigliotti@ensma.fr,

Keywords: Organic Matrix Composites (OMC), 3D Woven Composites, In-situ test, Acoustic Emissions, μ -Computed Tomography, Finite Element Model

Abstract

The present paper focuses on in-situ multi-axial testing of three-dimensional (3D) woven organic matrix composites for aeroengine applications. Damage onset is characterised by X-ray μ -Computed Tomography (μ CT) based in-situ tests, supported by Acoustic Emission (AE) analysis and by Finite Element (FE) simulations. The synergy between these techniques allows having knowledge of the solicitation at which damage onsets and defines the first points necessary for the construction of a damage onset surface at the sample scale.

1 – Introduction

The weight reduction of structures is a challenge in the field of aeronautics. Composite materials have been used since the 1970s for secondary parts of the aircrafts and they are now increasingly used for primary parts. Organic matrix composites (OMCs) reinforced with carbon or glass fibres are the most widely used. In the latest generations of aircrafts they are the most used type of materials for structural parts. However, even if composites have been used for the last 40 years in the external structural parts of the aircrafts, the current trend is to start using composites with complex microstructures (such as 3D woven composites) in more complex parts of the aircraft, such as structural parts of the engines, particularly first stages of the compressor blades.

When studying the mechanical behaviour of such kind of structures and particularly the damage mechanisms emerging at the material level two main issues arise:

- the complexity of the material at the mesoscopic and microscopic scale: 3D woven OMCs exhibit a complex heterogeneous microstructure/mesostructure, the interfaces between fibre and matrix, the different orientations between tows make more complex the understanding of the damage onset mechanisms,
- the complexity of the solicitation during service, different types of loads will act on structures: for instance for a fan blade, centrifugal forces which vary from the root to the tip, aerodynamic forces which depending on the fan shape, etc.

Aircraft and aeroengine manufacturers are particularly interested at the phenomenology and mechanisms of damage onset. Several techniques are deployed in order to study and characterize the damage in fibrous materials. One of the oldest is Acoustic Emissions (AE). Each energetic event in the material is a potential source of an acoustic wave. A large number of publications/communications since the last century have allowed correlating the signal parameters to the physical mechanisms of degradation ([1]-[8]). By multiplying the sensors it is possible to locate the events. However this measurement is often indirect and when the number of signals increases or when the material is highly absorbent, the technique shows several limitations. X-rays are a second possibility that probes the material in the 3D volume and the exploitation of the different levels of absorption allows to identify a change in morphology. X-rays were used in the 1990s to identify microcracking kinetics in damaged composite materials (see, for instance, [9]). The availability of X-ray tomography setup supported by powerful image analysis offered new tools to characterize the damage mechanisms. These systems can be used to analyze the damage after a specific load history (for instance, fatigue...), but when the load is removed in order to do the tomographic scan (so called *ex-situ* tests), cracks may close and be undetectable. The *in-situ* setup allows the opening of all cracks and the observation of the whole damage network. More recently [10-18], the use of *in-situ* devices has proved to have an interesting potential for monitoring damage but also changes in the shape of the microstructure, during loading. However, these techniques are limited by the accuracy of the X-ray beam and recorders [12]. Lowering the setup accuracy/resolution requires the use of large instruments. Some laboratory tomography devices allow micrometric accuracy/resolution, and provide information on the evolution of the damage mechanisms.

More specifically, these techniques have been used in CMCs under load and under the effect of the environment. Mazars et al. [10] investigated failure of a melt-infiltrated SiC/SiC composite at room temperature and at 1250°C in air. A damage scenario has been established with the help of numerical simulations. Bertrand et al. [11] investigated damage development during thermomechanical cycles and tensile loading by X-ray micro-computed tomography (μ CT) under scanning electron microscopy (SEM). Chen et al. [12] performed FFT simulations and micro-computed tomography (μ CT) observations during *in-situ* uniaxial tensile tests. A representation of the real microstructure, with a good description of the local microstructural geometry, is proposed, the location of cracks in tubular samples and the onset of damage are compared to FFT's simulations. This comparison shows that cracks preferentially initiates at tow interfaces, where the presence of sharp edges at macropores generates stress concentrations.

For organic matrix composites, e.g. Schöttl et al. [13] proposed an *in-situ* μ CT setup for cyclic load tests and observed the different stages of crack propagation during cycling loading. The parameters of the cracks were deduced by segmentation. With a composite torsion tube, Chai et al. [14] characterized the onset and propagation damage modes, quantifying the role played by the

reinforced tows. Wagner et al. [15] performed a similar study, *in-situ* X-ray computed tomography and stiffness evolution monitoring were used to study damage initiation and propagation in laminate composite samples subjected to tension-tension fatigue loading. These authors have established that a clear correlation can be found between the increasing number of matrix cracks and the observed stiffness degradation of the composite specimen.

Under a synchrotron beam the spatial resolution can be very high. For example, Watanabe [16] has studied crack initiation and propagation under applied load with a spatial resolution of ~ 50 nm. These results show that voids and cracks initiation are not only the result of local stresses but are also due to two competing nanoscale mechanisms, that is, fiber/plastic interface debonding and in-resin crack initiation. The mechanisms are described in function of the ply thickness. This information is very valuable for developing models at different scales.

This technique is also used with single-edge notched (SEN) samples, Jo et al. [17] applied this protocol to symmetric cross-ply laminate combining synchrotron X-ray tomography and Digital Image Correlation (DIC) technique at the micro- and macro-scales. The various fracture modes are identified and the authors observe many initial cracks sequentially occurring near the notch tip. Mechanical parameters are deduced by measuring the crack lengths and opening displacements from the 3D CT images at different loading steps and the stress relaxation is directly measured by DIC analysis using the macro-scale test data. This relaxation appears in the region between existing and emerging transverse cracks.

Hufenbach et al. [18] studied damage evolution in carbon fibre reinforced plastics (CFRPs) made of weft knitted and woven preforms and more precisely the behavior in thickness direction by using cylindrical tensile specimens according to ASTM D 7291. These authors use also compression specimens with different aspect ratios to study the compressive failure of CFRP woven composites.

Not much work has been carried out concerning multi-axial loadings applied to 3D woven composite [19]. Although many test have been proposed to achieve a multi-axial state in composite materials [20] various experimental complexities arise to avoid undesired phenomena like edge effect or high stress gradients. Moreover, studies of damage mechanisms during multi-axial loading [21, 22, 23] are still unusual; the present work aims to cover and add some knowledge regarding both multi-axiality and damage mechanism, highlighting the onset of damage.

This methodology allows assessing damage onset in of three-dimensional woven organic matrix composites. These tests are often carried out on small samples. However, in case of 3D composites – since their pattern characteristics can be close to one of the dimensions of the structure (thickness) – working with a representative volume can be a first challenge. Besides, the literature works often investigate only one loading path, limiting the aim of the results. In order to study damage onset it is important to test multi-directional loads and to capture *in-situ* the appearance of damage. Moreover, the development of damage onset criteria based on the assessment of damage onset mechanisms is needed. One of the main difficulties consists in identifying the time and the place of the first damages. As far as the place is concerned, X-ray tomography allow to do so, depending on its resolution. Synchrotron facilities enlarge the investigation range, but their implementation and access is limited. A good compromise consists in combining acoustic emission and tomography methods. *To our knowledge, there are not many tests coupling several types of loading with EA to identify the initiation of the first damage [19, 24, 25].*

The present paper focuses on *in-situ* multi-axial testing of three-dimensional (3D) woven organic matrix composites for aeroengine applications. *The proposed test to achieve such a multi-axial state is a traction/torsion. Combined load path generates different stress field in the meso-structure and it permits to study the link between stress field, local meso-structure and onset of damage.* Damage onset is studied with X-ray μ -Computed Tomography (μ CT) based *in-situ* tests, supported by Acoustic Emission (AE) analysis and by Finite Element (FE) simulations. The synergy between these techniques allows having knowledge of the solicitation at which damage onsets and defines the first points necessary for the construction of a simple macroscopic damage onset surface at the sample scale. The aim of the paper is to propose a first step towards the definition of a robust protocol to identify a damage onset criterion at the macroscopic scale. The identification of a microscopic onset criterion needs the development of dedicated tools, the identification of local properties and will be the object of further work.

The paper is organised as follows: Section 2 presents the material, the experimental setup and the model approach, Section 3 illustrates the experimental results. A complete analysis of the onset and localisation of first damage will be carried out, the correlation with AE and μ -tomography will be presented and a summary of all results will be given, Section 4 presents Finite Element Model results and propose a macroscopic onset criterion. Finally, Section 5 presents conclusions and perspectives.

2 – Material, experimental setup and model approach

In this part the materials, the experimental setup and methods and the model approach are presented. It is important to point out that a torsion-traction testing machine is installed on a tomography platform to perform *in-situ* tests. The metrology combines the measurement of loads (tensile and/or torsion), the displacement of the moving grips, tomography and acoustic emission.

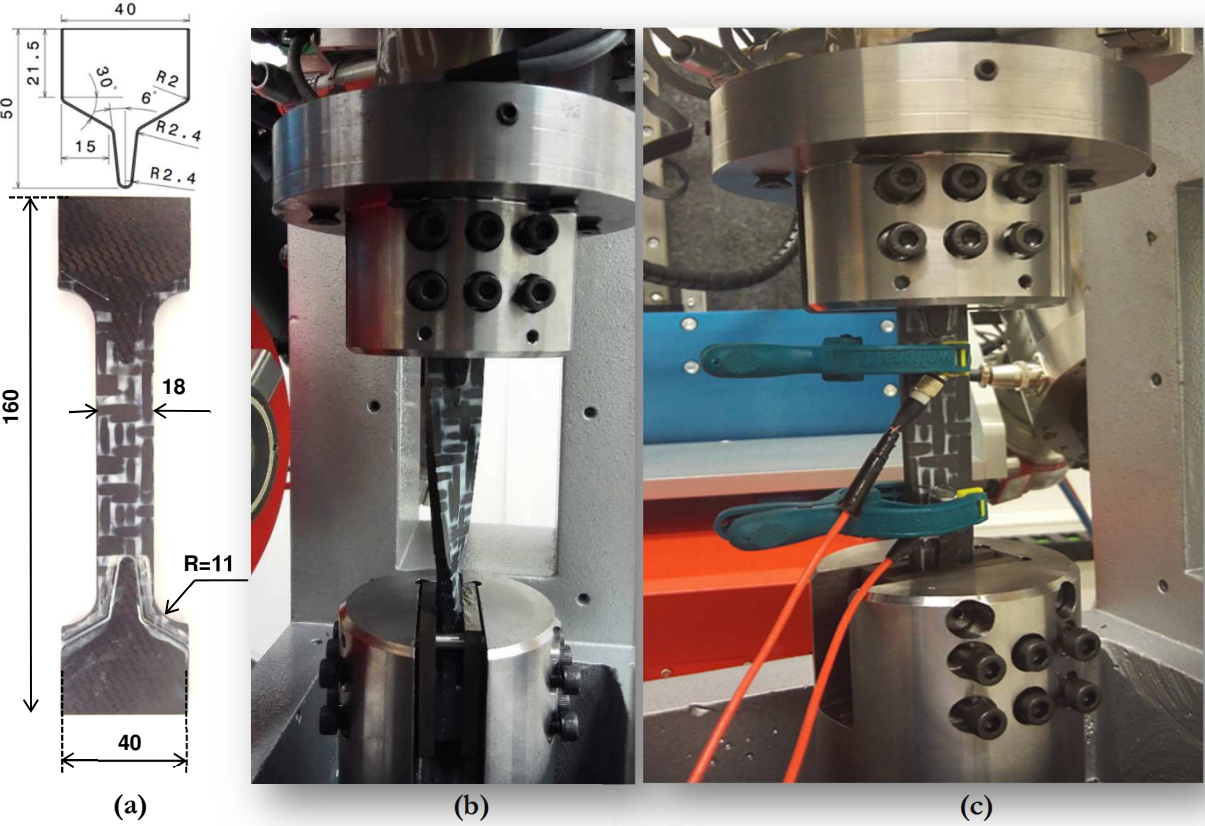
2.1 – Material and experimental setup

The 3D woven OMC materials samples are made by Resin Transfer Molding (RTM) manufacturing techniques and are provided by the industrial partner. A plate is cured with a process similar to that used by the industrial parts, pressure, temperature and time are identical. After curing the samples are cut with high pressure water jet. *At the level of the constituents, commercial HexTow® IM7 carbon fiber and CYCOM® PR 520 epoxy resin are used [26].* The architecture of the specimen provides a global anisotropic behaviour. Two different types of samples are employed: 4-ply and 8-ply samples. The thickness of 1 ply is around 1 mm. *The exact architecture of the woven fabrics and its global properties are not reported for confidentiality reasons.*

Fig. (1a) illustrates the sample geometry and the shape of grips tabs glued on the specimens heads. The role of the aluminium tabs is to avoid direct contact between the machine and the sample. This joint is a critical section which may undergo sliding during the test. The shape and design of aluminium tabs are optimised in order to allow better stress distribution in this critical zone and to avoid parasite stress concentrations during the test. *The choice of the specimen dimensions comprises two important strategies. The first of them concerns the length and shape of the specimen; it is necessary to reduce the stress concentration close to the grips and its propagation through the study section where multi-axial state claims to be studied. Also, the presented dumbbell shape, helps to mitigate that effect; previous finite element conception studies in straight bars did show that the most solicited area is close to the grips. However, in a dumbbell-shape specimen with a considerable relatively length it is possible to reduce this effect for the given length of the specimen (160mm) the parasite effect of the stress concentration due to grips can be neglected in the centre of the specimen. The second strategy concerns*

the width/thickness ratio. Concerning the thickness, it is fixed by the manufacturing process. The choice of 18 mm is made paying attention at the maxim shear stresses generated while twisting.

Fig. 1b illustrates a deformed sample under torsion and the links with the grips, it is possible to observe the pointed end of the tab protruding from the clamping elements. During loading acoustic emissions are recorded. The position of AE sensors are shown in Fig. 1c.





(d)

Fig. 1: (a) Sample and grips used in experiments with dimension in mm and description of grips tabs (Aluminium), (b) Sample after pure torsion test, (c) Mounting of the sample with the recording sensors installed on the surface, (d) Experimental setup for micro-tomography scan.

The setup used for this study allows applying traction-compression coupled with torsion loading. The machine developed by RX-solutions is specifically designed to allow mounting inside the tomograph. In addition, the two upper and lower grips can be rotated through 360° in order to produce X-ray images. The parallelism and concentricity of the two jaws must be perfectly achieved before the experiment in order to obtain the desired quality in the images but also to avoid adding a parasitic load during the synchronized rotation. The maximum level of traction force is equal to 25 kN, the maximum torque is 100 Nm, the amplitude of longitudinal displacement is equal to 50 mm and the amplitude of the rotation angle is not limited since rotating electrical connectors are used.

The setup frame used to apply the load (traction-compression and/or torsion) is clamped on top of the rotation stage framework by bolts, while the rotation plate of XR tomograph is deactivated. The protocol consists in applying a displacement and/or rotation ramp through the mobile head with a selected speed. The test is interrupted several times during the experiments. During the interruptions, the displacement is kept constant and both grips rotate slowly maintaining their relative positions. μ CT scans of the specimen are recorded during that time. In addition, the load can evolve during acquisition steps due to material relaxation. The choice of the loading level at interruptions depends on the AE activity. This point is important since it allows to identify damage onset.

The multiaxial testing protocol consist in a tensile or compression test immediately followed by a torsion test. In order to conduct multiaxial tests, a first tensile test was conducted on a 4 mm thickness specimen in order to identify the onset of the first damage using AE. Results showed that stress level associated at the onset of the first damage is

around 205MPa. A further 3D image of the cross-section before and after tensile testing showed an intra-tow crack at the length where AE was recorded. Hence, the decided protocol consist in a first tensile test below the first damage onset stress level found (205MPa). This stress states will be set on 52MPa and 104MPa, which are a quarter and a half the onset in tensile test. According to the sample cross-section, the associated forces to achieve such a stress state in the tensile machine will be 7.1kN and 14.2kN respectively. These forces are measured by the machine device and a speed displacement of 1mm/s is imposed. In order to fit a symmetric first envelope, same protocol with same stress sates and forces in compression configuration.

A two-channel PCI-2 from Mistras Group is used to record AE signals during tensile tests. The test is carried out with two Micro80 piezoelectric acoustic sensors (100 kHz–1 MHz bandwidth - 10 mm diameter) with a PAC1220 A preamplifier with a gain of 40 dB. The sensors are positioned on the specimen with silicone grease and held by a clamp (Fig. 1c). When recording AE signals, the user sets a detection threshold (35 dB) below which no signal is recorded. The amplitude distribution is 0–100 dB (0 dB corresponds to 1 mV at the transducer output). The acquisition system is calibrated before each test using the mine breakage procedure [1, 2]. The test allows estimating the propagation velocity and attenuation of acoustic waves in the material, which is 2000 m/s. It should be noted that the elastic waves detected by the AE sensors and converted into a useful signal are also called hit. The characteristics of a signal such as duration, rise time and amplitude are recorded over time. Using two sensors, the setup enables linear location of AE signals along the gauge length of the specimen.

In order to validate the protocol, a preliminary study about the identification of noise sources has been carried out before testing. Since the stepper motors of the in-situ machine represent potential sources of noise, tests on the in-situ machine placed on the floor were carried out. First, a steel test piece was clamped into the two grips, an AE sensor was placed on the surface of the sample and the synchronous rotation of the two motors was imposed to simulate the movement of the motors during scan. The same was done by clamping the specimen only in the lower grips to reproduce the movement of the grip during the torsion test. In both cases, the amplitude of the signals did not exceed 25-28dB, a noise that could be related to the electrical noise of the signal preamplifiers, but also to the surrounding environment or displacement, rotation or slide of the grips. This level of noise should not interfere with composite testing since the magnitude of AE for matrix cracks in C-epoxy composites is in the range between 40 and 70dB. Table 1a reports the parameters of the AE setup.

AE acquisition hardware parameters		μ CT acquisition parameters	
Gain [dB]	40	Source [kV]	150
PDT [μ s]	300	Voltage [kV]	60
HDT [μ s]	600	Current [mA]	166
HLT [μ s]	1000	Imageur [px^2]	1920x1536
<i>Duration [ms]</i>	<i>1000</i>	Nb Images	10

Threshold [dB]	30	Frame rate	1.15
Sound velocity (m/s)	2000	SOD [mm]	107.135
		ODD [mm]	965.865
		Duration [hours]	4
		Resolution [$\mu\text{m}/\text{vox}$]	13

Table 1: AE acquisition hardware parameters and μCT acquisition parameters.

The main aim of the μCT scan is to obtain a 3D image of the net specimen, detailed and fast enough to reduce the time of use of the tomography for each test on one side and reduce the effects of relaxation of the material on the other side. For each rotation of the specimen during the scan, the acquired image is the result of an average of several images taken for the position of the specimen at a given time. Many averages between images would lead to longer scans; on the contrary, a low average image would lead to untidy the images.

The distance between the specimen and the X-ray generator (Source Object Distance - SOD) and the distance between the specimen and the sensor (Object Detector Distance - ODD) are parameters that will affect directly the resolution of the image. For well clear-cut and high-quality results, the SOD should be reduced as much as possible considering the limitation of the presence of the test machine. The ODD should be increased as possible considering the exposure time. Table 1b reports the parameters used for μCT scans.

Fig. 2 schematically illustrates the dimensional parameters of interest: the position of sensors in the sample and the length of the by μCT scanned zone, considering the limitations of the acquisition system. Fig. 2 is important since it allows finding the exact position of damage onset by cross-referencing the information from tomography and from the acoustic emission sensors.

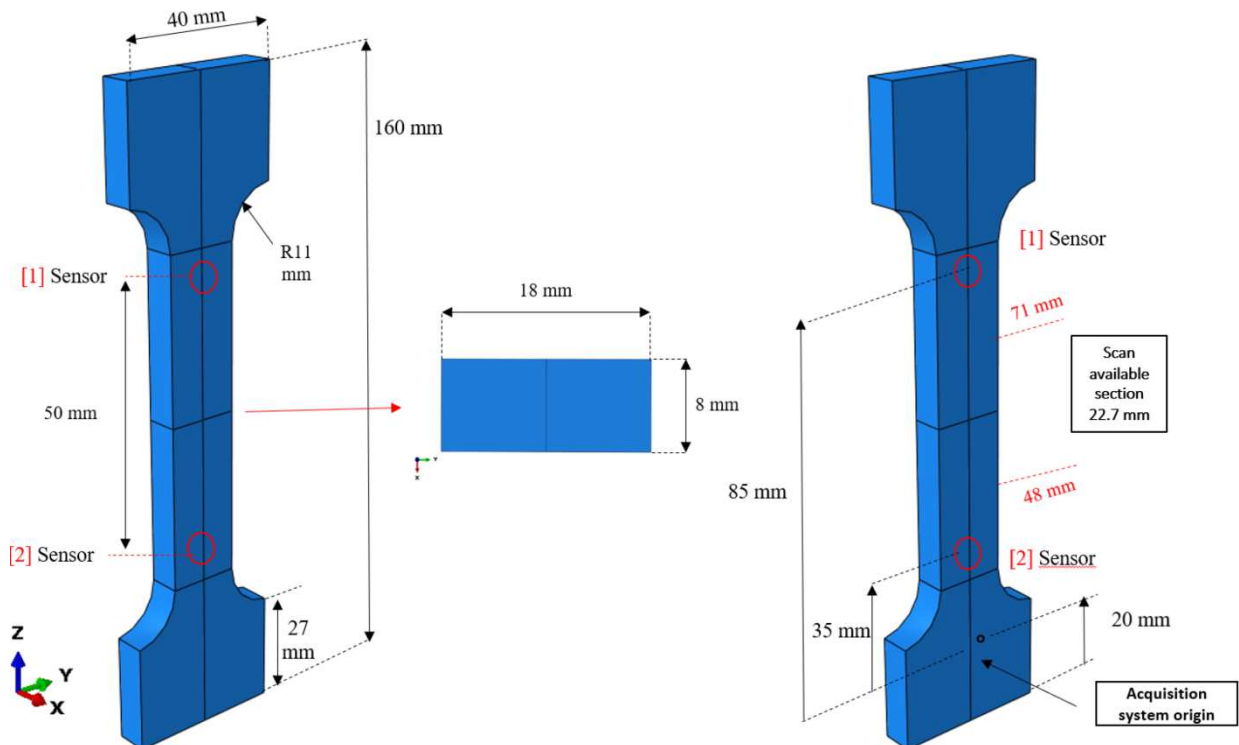


Fig. 2: AE sensor position scheme and used coordinate reference system.

With this system it is therefore possible to study the stiffness of the composite as well as the onset and evolution of damage in the 3D material at the scale of the fibrous tow. The variable parameters are the loading path (torsion, combination of tension-torsion compression), the level of the loading components, as well as the thickness of the specimen and therefore the number of patterns in the sample. Table 2 summarizes all the performed tests: an acronym is defined in order to facilitate the analysis of results.

Experiment	Acronym	Thickness
Pure Torsion 8 ply	P-T-8	8 Ply
Pure Torsion 4 ply	P-T-4	4 Ply
Traction [52MPa] + Torsion 8 ply	T[52]-T-8	8Ply
Traction [52MPa] + Torsion 4 ply	T[52]-T-4	4Ply
Traction [104MPa] + Torsion 8 ply	T[104]-T-8	8Ply
Traction [104MPa] + Torsion 4 ply	T[104]-T-4	4Ply
Compression [104MPa] + Torsion 8 ply	C[104]-T-8	8Ply
Compression [104MPa] + Torsion 4 ply	C[104]-T-4	4Ply

Table 2: Summary of the performed tests.

This experimental scenario should be rich enough to see the effect of multiaxiality in the material response.

2.2 – Model approach

In order to assess the homogeneous macroscopic state of the stress induced in the sample by the test presented above, a very simple numerical model has been developed. The model schematizes the composite material by an anisotropic equivalent homogeneous medium, at the sample scale. The macroscopic calculated quantities (strains/stresses) can be used within engineering failure and design criteria.

The specimen is represented by 3D elements, the shape reproduces the mean dimensions measured on the samples. Fig. 3 represents a scheme of the sample FE model geometry, as well as boundary conditions and loads. An attempt has been made to reproduce as faithfully as possible the original experimental conditions. The sample has been blocked in all possible displacements and rotations at the bottom grip while the load has been imposed at the top grip. Interaction constraints between all the grip nodes have been imposed in the grip zone. The mesh consists only of linear hexahedral elements with reduced integration in order to limit the time of calculation. A study of mesh convergence has been performed to verify the quality of density of this mesh. A compromise has been chosen between time of calculation and precision of numerical solution. The main material orientations is defined as follows: longitudinal direction of sample corresponds to the warp direction (longitudinal tows), transverse direction correspond to the weft direction (transversal tows), and in

the thickness direction the 3D reinforcement (through-the-thickness tows). The properties of the 3D woven laminate are orthotropic; the exact material properties are not reported for confidentiality reasons. On the other side, the tabs are connected to a master point with an assumption of kinematic rigid displacement. The angle of twist (longitudinal axis) is imposed and varies linearly and the torque is measured at reference point. For coupled situation, angle and longitudinal displacement are applied on the reference point in the same protocol of experimental procedure.

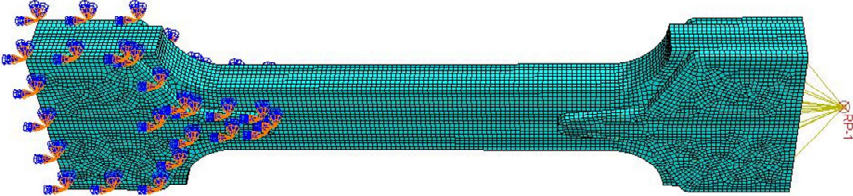


Fig. 3: Geometry, mesh and boundary conditions of macroscopic model

3 – Experimental results

In Fig. 4 the global responses in torsion, coupled traction-torsion and compression-torsion are reported over the entire load range. The torque is plot as a function of the rotation angle imposed during the tests, the two interruption test angles (1st stop, 2nd stop) are indicated by black dotted lines. The response of 4 ply and 8 ply samples are similar, the torque values are higher for 8 ply. It can be seen that in the very beginning the behaviour is linear, then, as the torque-strain is increased, the non-linearities start to appear early. This non-linear behaviour is due to the viscoelasticity of the matrix, onset of damage and damage propagation. During the stops, some recovery is observed, due to matrix viscoelasticity and to the effect of the internal architecture of tows on the mechanical response. At the first stop under pure torsion the torque decreases from 23.8Nm to 19.8Nm for 8 ply samples, and from 5.5Nm to 4.8Nm for 4 ply samples. This recovery is approximately equal to 16.8% for 8ply and 13.6% for 4ply. Both kinematics of relaxation are in the same order in magnitude for an identical interval of time.

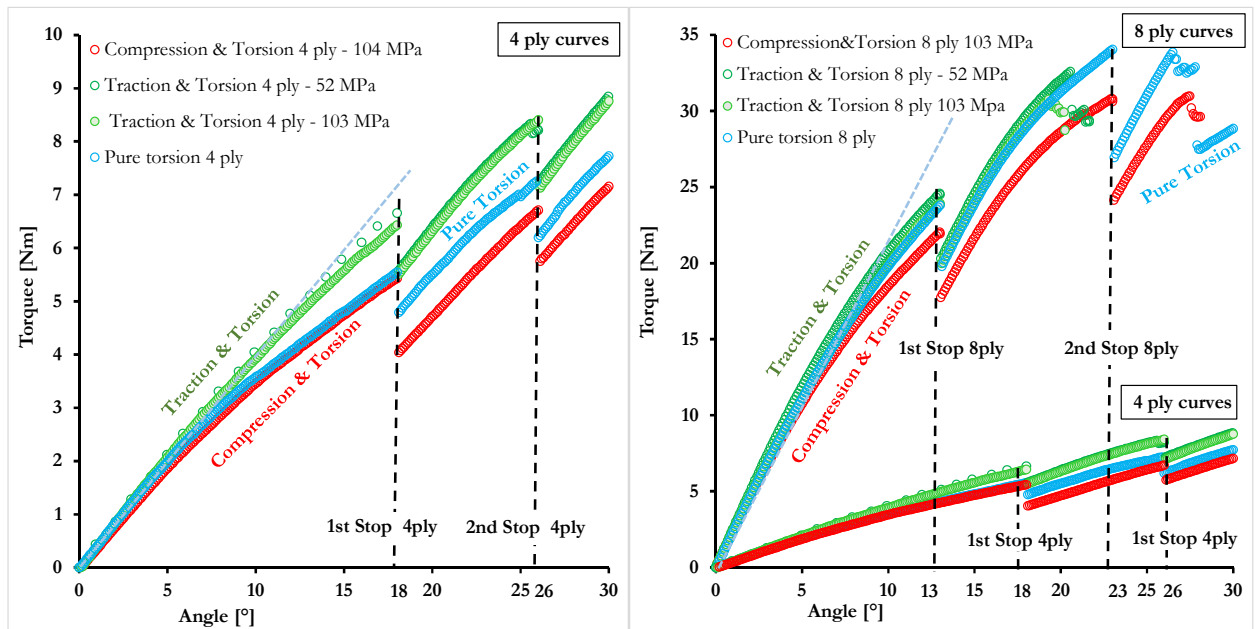


Fig. 4: Torque-twist angle curves for all tests. Interruptions have been marked with black dotted lines.

As expected, the initial slope of the curve is affected by a traction load, and stiffness increase could be related to a tow alignment effect. The modification of the architecture is of the second order on the stiffness but its effect is quantifiable when compared to the original slopes. In compression-torsion the effect is reversed. At this stage of the study, these macroscopic data do not allow for any conclusions to be drawn, but the sensitivity on the global stiffness allows differentiating the effect of combined loads.

3.1 – Coupled AE- μ CT analysis for the identification of damage onset

Fig. 5 illustrates AE events (of amplitudes higher than 30 dB) during loading for the P-T-8 test.

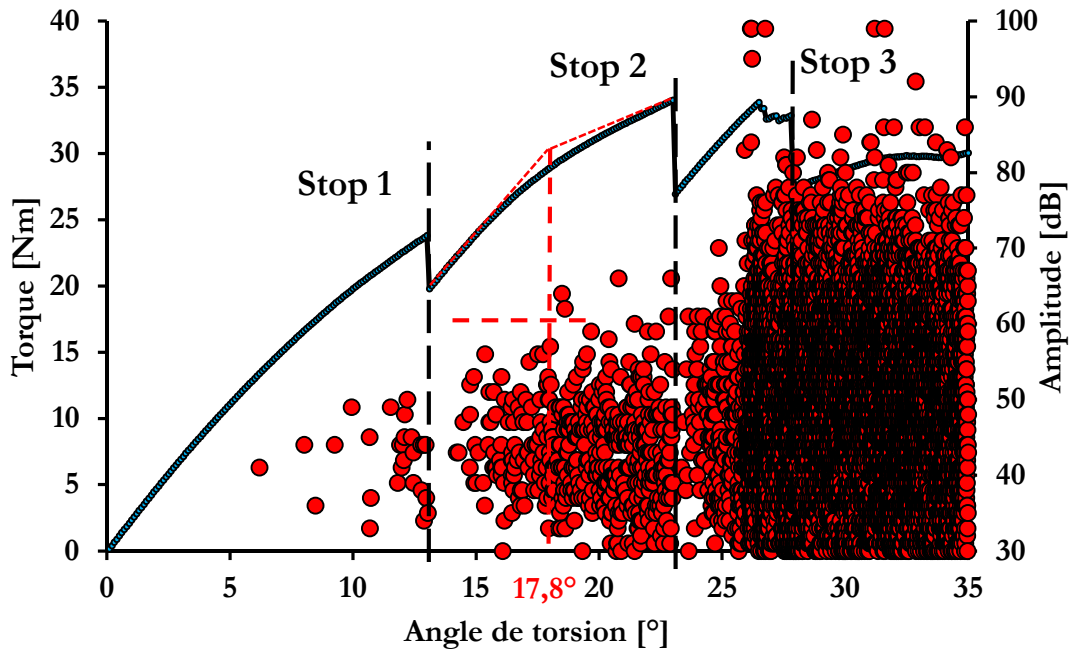


Fig. 5: Torque-twist angle curve for the P-T-8 test. Interruptions have been marked with a black dashed line. AE events in red circles are superposed to the curve.

A scarce AE activity is noted before the first test interruption, Stop 1. The amplitudes of the AE events are small corresponding perhaps to small matrix or interface cracks. Moreover, a close observation of the images recorded during stop 1 does not show any damage ($13 \mu\text{m}/\text{vox}$). This does not indicate that this process has not started, but that if it exists, it is less than 13 microns. The stiffness has decreased without AE activity, this point allows associate this stiffness decrease with viscoelasticity before Stop 1. Between Stop 1 and Stop 3 viscoelasticity and damage both contribute to stiffness decrease.

Regarding the scanning time at interruptions, a trade-off between the viscoelastic relaxation phenomena during the stop, which inherently has a stress reduction for the imposed strain, and the set of tomographic parameters (described in section 2.1 – Material and experimental setup) responsible of a quality and clear image at whose resolution damage may be observed. Advanced image processing techniques during acquisition allows to deal with artefacts of a material nature (such as viscous relaxation), but also related to the own acquisition process. The scanning time comprises 2h approximately, sufficient to have a quality image and mitigate as far as possible the viscosity effects.

Stronger AE activity is recorded between Stop 1 and Stop 2 and then between Stop 2 and Stop 3. The very dense AE activity recorded after 25° twisting angle, associated with a notable and abrupt change of the loading curve, clearly indicates the development of severe damage, with significant loss of sample torsional stiffness.

Since in the present work is focused on the damage onset, the events after the second stop are ignored and all the attention is focused on the events occurring between Stop 1 and Stop 2. The aim now is to select the angle corresponding at the onset of visible damage, to determine the area and to quantify the type and shape of these damages. In order to select this angle, two parameters were crossed: firstly: the amplitude of the acoustic events, which increases as the angle increases, and secondly, the loss of rigidity. In Fig. 5 it appears that the first events exceeding 60 db correspond to an inflection point of the curve (dotted red lines). Such amplitudes are a sign of major energy events

within the material. The way this angle is determined – as well as the section at which onset takes place – is described in the following paragraphs by carrying out a coupled analysis of AE events and μ CT observation.

Fig. 6 illustrates localized AE events as a function of time and space in a sample zone between 48mm and 71mm from the bottom sample, this is the zone where the μ CT scan is carried out: loading between Stop 1 and Stop 2 takes place between 10s and 110s, the test is then stopped at 110s and the scan at Stop 2 is carried out up to around 250s. It is useful to remind (see Fig. 6) that the piezoelectric sensors are placed 50 mm from each other, but the μ CT scan length is around 23 mm.

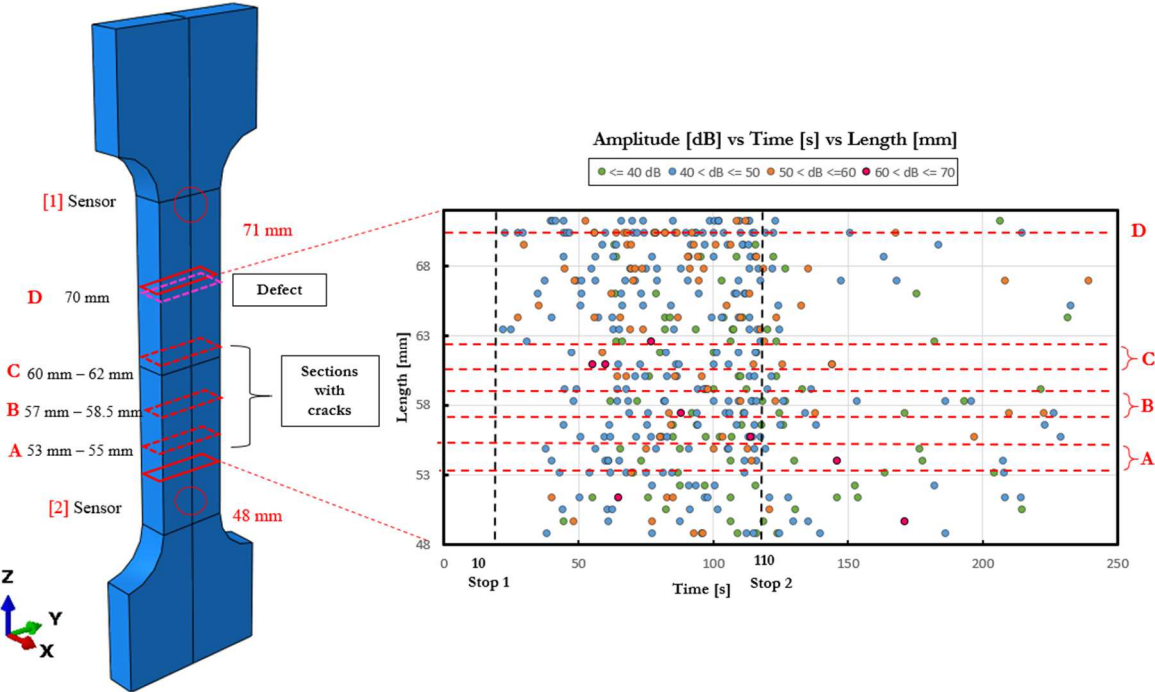
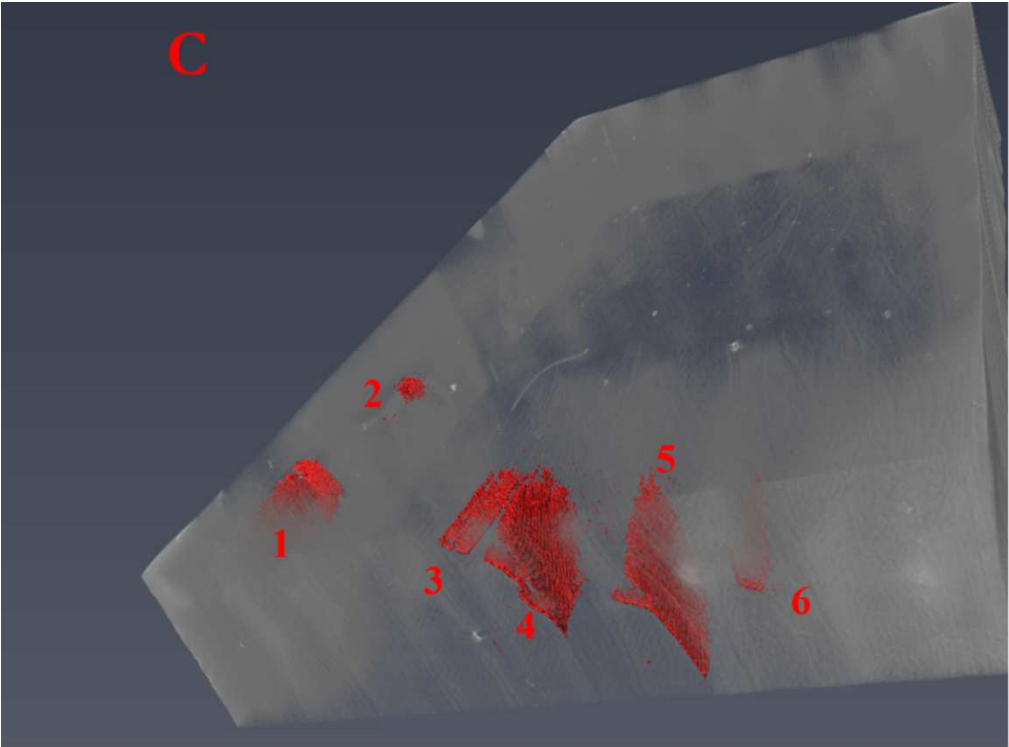


Fig. 6: AE events in the μ CT scanned zone as a function of time (P-T-8 test) and by AE / μ CT correlation identification of critical cracked zones within the sample.

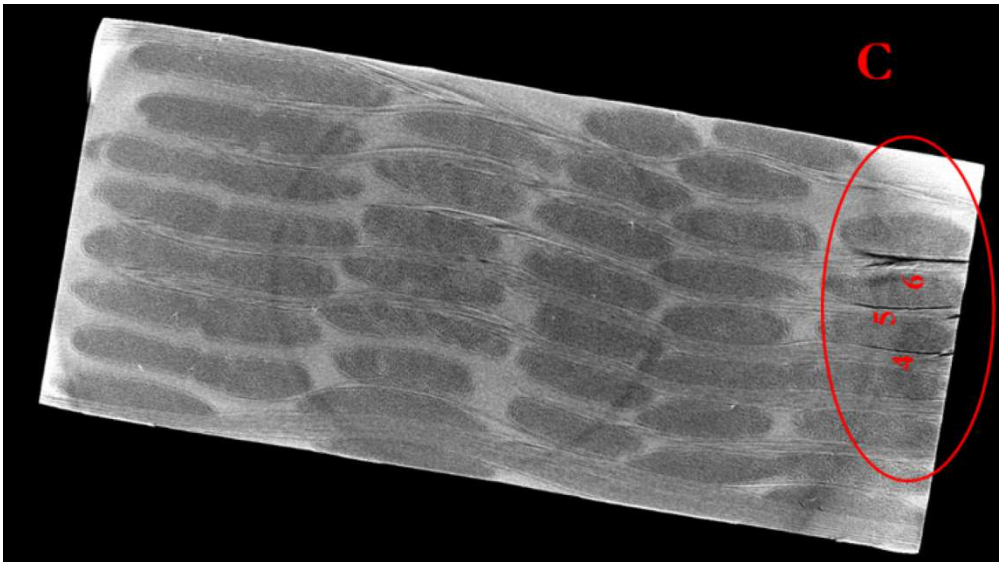
In Fig. 6 the AE events are discriminated on the basis of their amplitude. Green circles indicate AE events whose amplitude is higher than 30 dB (which can be taken as a noise threshold) but lower than 40 dB, blue circles indicate AE events whose amplitude is between 40 dB and 50 dB, yellow circles indicate AE events whose amplitude is between 50 dB and 60 dB, red circles indicate AE events whose amplitude is between 60 dB and 70 dB. High amplitude events are clearly related to damage events. Here no empirical classification or correlation of AE events ([1, 2]) is carried out, but AE events are directly correlated with damage observation carried out during in-situ μ CT scans.

Fig. 6 identifies potential damaged zones (A, B, C, D) in which AE events have high amplitude (clusters of yellow or red AE events).

By analysis of μ CT scans it is possible to find that zone D corresponds to a zone with a pre-existing defect (an inclusion), therefore the AE activity in this zone is related to propagation of damage starting from a defect due to the manufacturing process and localized with RX. Though explaining the role played by small defects on damage onset, this information is not of interest in this specific study and will be ignored. Zones A, B and C (between 53mm and 60mm) contain similar clusters of cracks.



(a)



(b)

Fig. 7: (a) 3D and (b) 2D rendering of μ CT scan along the critical Zone C (P-T-8 sample).

A tomographic scan performed at Stop 2 in Zone C between 60 mm and 62 mm (3D and 2D rendering, Fig. 7 reveals the presence of several cracks (cracks numbered from 1 to 6) of small/average length which have onset close to the external edge during loading between Stop 1 and Stop 2. These cracks are mainly inter-tow-type cracks (matrix-tow debonding at tow/matrix interfaces and tow/tow interfaces) spanning along the sample width and length direction. Table 3 resumes some useful morphological information about these cracks, specifying crack 3D area, surface and type.

Crack	Area 3D [px ²]	Surface[mm ²]	Type
1	17164	1.4	Intra-tow
2	2218	0.18	Intra-tow
3	6030	0.51	Inter-tow
4	30794	2.6	Inter-tow
5	28614	2.4	Inter-tow
6	8399	0.71	Inter-tow

Table 3: Surface crack parameters in the most critical section (P-T-8 sample).

This information gives a good idea about the location of damage onset in the P-T-8 sample.

The exact space and time location of damage onset can be found by looking at a chart of space and time cumulative AE events (Fig. 8).

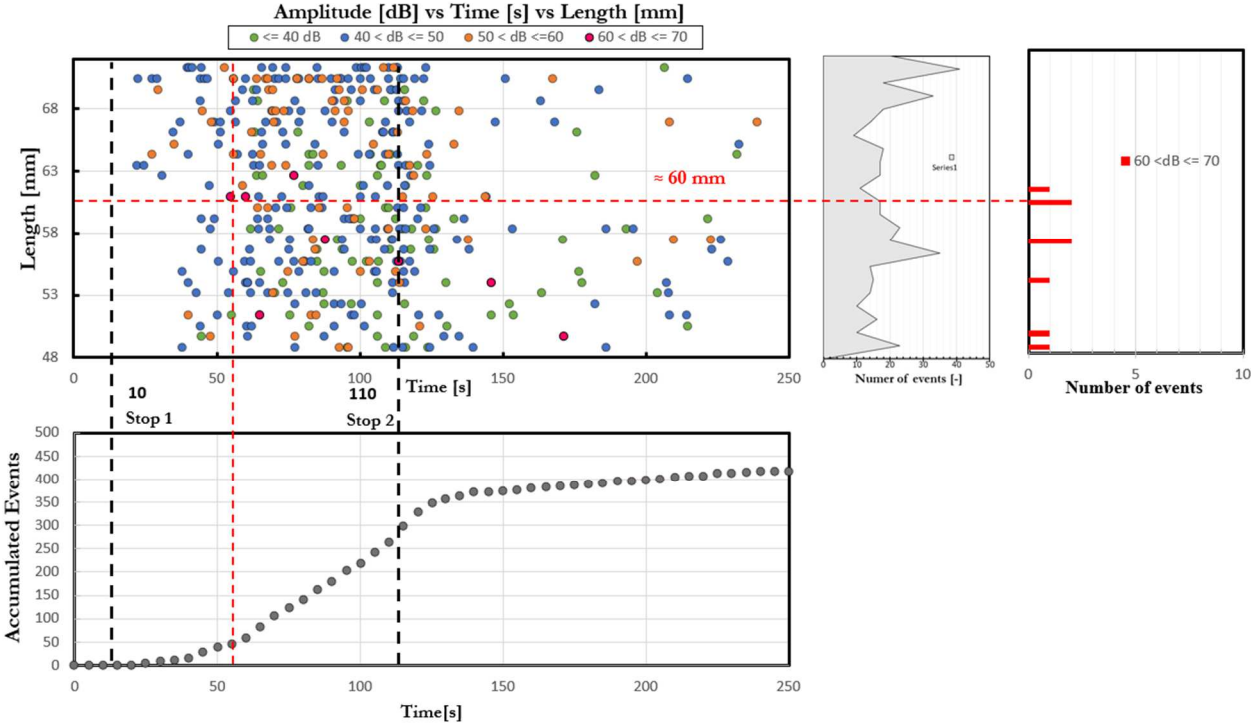


Fig. 8: By AE / μ CT correlation identification of onset time and location (P-T-8 test).

The intersection between the line at which the time cumulated AE events start rising (vertical red dotted line in Fig. 8) and the line indicating the critical section identified by μ CT analysis (horizontal red dotted line in Fig. 8) gives a good indication of the time (around 60s) and section (around 60 mm) at damage onset. The onset time corresponds to the onset twisting angle of 17.8° indicated in Fig. 5.

It is interesting to note that a detailed analysis of the μ CT scan carried out at Stop 2 lead to find out that:

- 91 % of cracks observed in the entire sample are inter-tow type
- 9 % cracks are intra-tow type

Damage localisation along the specimen length is very similar for all solicitations. Damage onset is related to the torsional constraint between the matrix and the yarns. *Addressing the effect of different thicknesses and multi-axiality in the damage mechanisms types, it has been observed a slightly increase in the intra-tow crack type for minor thicknesses (18% of cracks P-T-4 case were intra-tow type) as well as for pre-loaded traction configuration, test in which the amount of intra-tow cracks were: 13% in T[52]-T-8 case; 12% in T[52]-T-4 case; 23% in T[104]-T-8 case. In can be also appreciated how the effect of increase the initial load leads to a major apparition of cracking inside the yarns. With respect the pre-loaded configuration in compression (0% of cracks C[104]-T-8 case were intra-tow type) it has been reported an apparition of intra-tow crack type when thickness is reduced. (9% of cracks C[104]-T-4 case were intra-tow type)*

3.2 – Review of experimental results

The analysis carried out on the P-T-8 sample and presented in Section 3.1 has been performed for all samples. Results are collected in Table 4.

Test	Acronym	Angle[°]	Section [mm]
Pure Torsion 8 Ply	P-T-8	17.8	60
Traction[52MPa] – Torsion 8 Ply	T[52]-T-8	16.3	53
Compression [104MPa] – Torsion 8 Ply	C[104]-T-8	17.5	58
Pure Torsion 4 Ply	P-T-4	34	69
Traction[52MPa] – Torsion 4 Ply	T[52]-T-4	30.5	67
<i>Traction[104MPa] – Torsion 4 Ply</i>	<i>T[104]-T-4</i>	<i>24.7</i>	69
Compression [104MPa] – Torsion 4 Ply	C[104]-T-4	30	64

Table 4: Summary of damage onset (angle and location) identified for all tests.

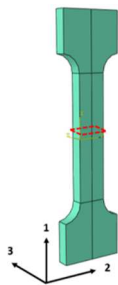
With the methodology illustrated in Section 3.1, for each sample, onset angle and section are determined. It can be seen that with respect to pure torsion samples (both 8 ply and 4 ply) the presence of a traction / compression solicitation simultaneously to torsion slightly decreases the

angle onset. First damage onsets always is inside the observed specimen zone, this point allows validating the setup and the proposed protocol.

4 – Finite Element Model results, correlation with AE and μ -tomography

According to the results of the analysis carried out in Section 3, for the P-T-8 sample the onset angle is located at 17.8 degrees, which gives a torque of around 33.5 Nm.

With this load value it is possible to calculate the homogeneous macroscopic stress field at the critical section (60 mm for P-T-8 sample) and to correlate this calculation with the observed μ CT damage. Fig. 9 represents the stress field, particularly S11, S12 and S13 components of stress (the most significant components of stress, for this type of sollicitation) in a zone close to the where damage is observed. (Direction 1 is the longitudinal direction, while 2 and 3 are transverse directions as schematized in Fig. 9). The stress tensor components values have been calculated at the integration points of those elements which are close to damage observed by μ CT (cracks from 1 to 4). Since the cracks are located in zones where the stress gradient is high, the maximum values are selected, and are collected in Table 5. These values can be considered as macroscopic failure stress values at damage onset. It is important to highlight that the size of the gradient is similar to the scale of the microstructure. A modelling study at the mesoscopic scale is therefore necessary.



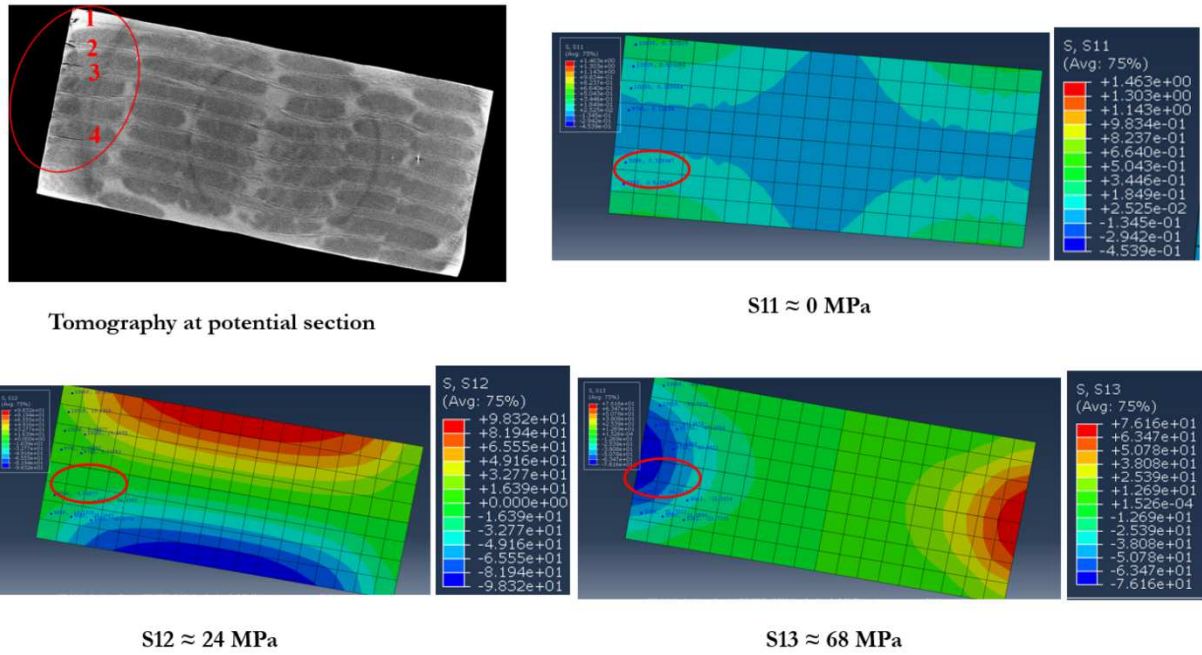


Fig. 9: Global sample FEM simulations (significant stress tensor components) in the critical section at damage onset (P-T-8 test).

Crack	S11 [MPa]	S12 [MPa]	S13 [MPa]
1	≈ 0	≈ 19	≈ 20
2	≈ 0	≈ 10	≈ 51
3	≈ 0	≈ 15	≈ 68
4	≈ 0	≈ 24	≈ 60

Table 5: Summary of stress values calculated by the global sample scale model at the most critical locations in correspondence with cracks observed by μ CT (P-T-8 sample).

By performing the same analysis for all tested samples, it is found that most of the cracks at the onset are in zones where S13 maximum values are calculated and most of the S13 values range from 50 to 70 MPa. On the other hand, the S12 values range from 10 to 30 MPa.

Fig. 10 summarizes, for all samples, the result of this analysis in the form of failure charts in the S11-S13 (Fig. 10a) and the S11-S12 (Fig. 10b) plane. The point in the charts can be used to identify a failure envelope (dotted lines in Figs. 10a and 10b) for the equivalent homogeneous material at the sample scale.

This value compares well with strength values of the CYCOM® PR 520 resin [26]. However a further comparison has to be done taking into account the meso-scale interaction between matrix and tows for more reliable results.

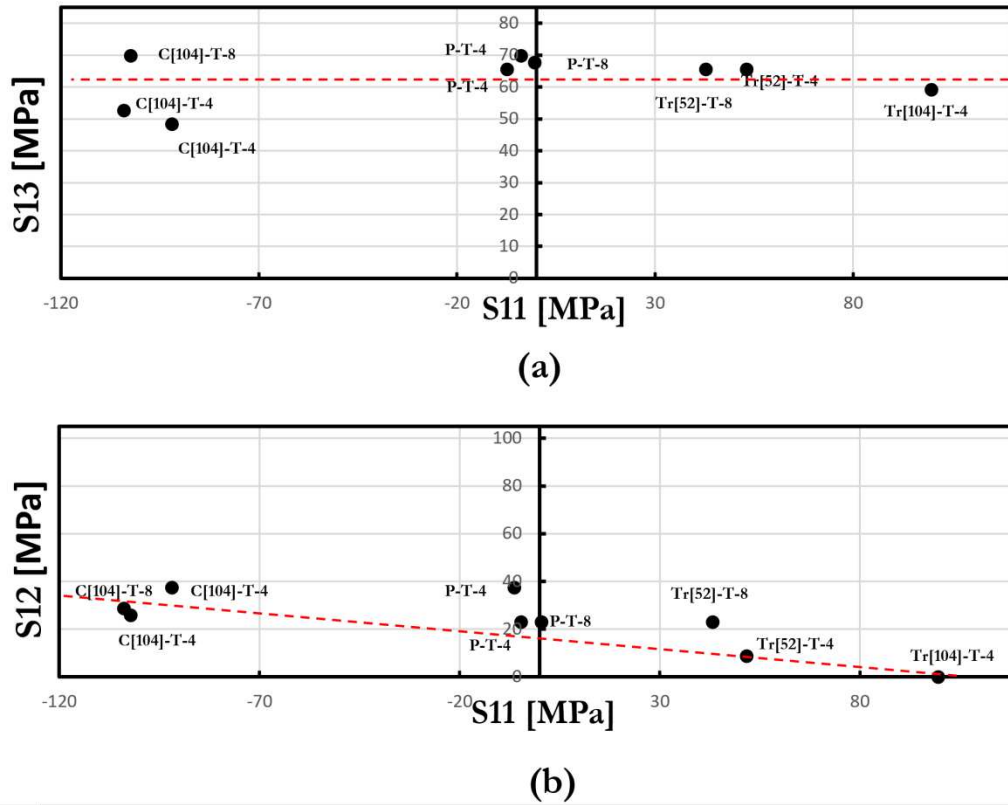


Fig. 10: (a) Critical stress and homogeneous failure envelope in the S11-S13 plane, (b) Critical stress and homogeneous failure envelope in the S11-S13 plane (P-T-8 test).

It is important to remark that the level of stress is overestimated, since the material behaviour is supposed to be linearly elastic, taking into account the effect of viscoelasticity stress values should decrease. However, this effect should not modify the conclusion on the failure surface. Taking into account the effect of anisotropic viscoelasticity with intra and inter-tow damage will be the object of further work.

5 – Conclusions

The present paper has been focused on in-situ multi-axial testing of three-dimensional (3D) woven organic matrix composites for aeroengine applications. Damage onset has been characterised by X-ray μ -Computed Tomography (μ CT) based in-situ tests, supported by Acoustic Emission (AE) analysis and by Finite Element (FE) simulations. The synergy between these techniques has allowed having knowledge of the sollicitation at which damage onsets and defines the first points necessary for the construction of a damage onset surface at the sample scale to establish an onset of damage or the studied 3D OMC. The main ideas and conclusions are highlighted below:

- In order to assess the damage mechanisms in complex structures such as 3D OMCs, which are also subjected to complex load phenomena, specific tests are needed to track the in-situ material response: complementary AE and tomography μ Scan tests allow to detect damage activity in time and space.

- It is possible to correlate the acoustic activity with the observed damage: those high amplitude events were correlated with the presence of cracks in the sample.
- It is possible to establish a time for the first damage taking into account the cumulative acoustic events, which is linked to the in-situ released energy during load. In this way, the onset time has been established for each test, which lead to a specific stress-strain configuration which permits to obtain mechanical information using FEM tools.
- The nature of the first damage has been quantified using μ CT scans. Morphology, surface, orientation and type of presented cracks has been evaluated leading to important results: around 80 % of the damage is given by inter-tow-type.
- It is possible to extract the stress field at damage onset using FEM codes in order to provide a failure onset envelope.

Since the AE and μ CT scans analyses are consistent, efforts must be focused on developing more accurate FEM models which should be taken into account:

- The effect of relaxation phenomena occurring during test interruptions: the current homogeneous model does not consider viscoelastic behaviour which leads to reduction in the stress while the load is taking place. By addressing this mentioned effect, FEM results would be more accurate.
- The effect of the heterogeneity can be implemented for each experiment in order to construct an onset criterion at the matrix level.

Acknowledgements

The work was funded by SAFRAN Composites. The authors acknowledge SAFRAN Composites for providing the material under study. The research subject falls within the research themes of the French Government program “Investissements d’Avenir” (LABEX INTERACTIFS, reference ANR-11-LABX- 0017-01, EQUIPEX GAP, reference ANR-11-EQPX-0018). PPRIME Institute gratefully acknowledges “Contrat de Plan Etat - Région Nouvelle-Aquitaine” (CPER) as well as the “Fonds Européen de Développement Régional (FEDER)” for their financial support to the reported work.

Data Availability Statement

The raw/processed data required to reproduce these findings cannot be shared at this time as the data also forms part of an ongoing study and for confidential reasons.

References

[1] Nielsen A. (1980), Acoustic emission source based on pencil lead breaking, The Danish Welding Institute Publication, 80, 15-20.

- [2] Eitzen D., Wadley HN. (1984), Acoustic emission: Establishing the fundamentals, *Journal of Research of the National Bureau Of Standards*, 89, 75-100.
- [3] Uenoya T. (1995), Acoustic emission analysis of interfacial fracture of laminated fabric polymer matrix composite, *Journal of Acoustic Emission*, 13, 95-102.
- [4] Caladro A., Esposito C., Lizza A., D'Amore A., Nicolais L. (1997), An acoustic emission characterization of the failure modes in polymer - composite materials, *Composite Science and Technology*, 58, 1923-1928.
- [5] Jemielniak K. (2001), Some aspects of acoustic emission signal preprocessing, *J. Mater. Proc. Tech.* 109, 242-247.
- [6] Godin N., Huguet S., Gaertner R. (2006), Influence of hydrolytic ageing on the acoustic emission signatures of damage mechanisms occurring during tensile tests on a polyester composite: Application of a Kohonen's map, *Composite Structures*, 72, 79–85.
- [7] Scholey J.J., Wilcox P.D., Wisnom M.R., Friswell M.I. Quantitative experimental measurements of matrix cracking and delamination using acoustic emission, *Composites Part A*, 41, 612–23.
- [8] Momon S., Godin N., Reynaud P., R'Mili M., Fantozzi G. (2012), Unsupervised and supervised classification of AE data collected during fatigue test on CMC at high temperature, *Composites Part A: Applied Science and Manufacturing*, 43, 254–60.
- [9] Lafarie-Frenot M.C., Ho N.Q. (2006), Influence of Free Edge Intralaminar Stresses on Damage Process in CFRP Laminates under Thermal Cycling Conditions, *Composites Science and Technology*, 66, 1354–1365.
- [10] Mazars M., Caty O., Couégnat G., Bouterf A., Vignoles G.L. (2017), Damage investigation and modeling of 3D woven ceramic matrix composites from X-ray tomography in-situ tensile tests, *Acta Materialia*, 140, 130-139.
- [11] Bertrand R., Caty O., Mazars V., Denneulin S., Rebillat F. (2017), In-situ tensile tests under SEM and X-ray computed micro-tomography aimed at studying a self-healing matrix composite submitted to different thermomechanical cycles, *Journal of the European Ceramic Society*, 37, 3471-3474.
- [12] Chen Y., Gélébart G., Chateau C., Bornert M., King A. (2019), Analysis of the damage initiation in a SiC/SiC composite tube from a direct comparison between large-scale numerical simulation and synchrotron X-ray micro-computed tomography, *International Journal of Solids and Structures*, 161, 111-126.
- [13] Schöttl L., Kolb P., Liebig W. V., Weidenmann K.A., Elsner P. (2020), Crack characterization of discontinuous fiber-reinforced composites by using micro-computed tomography: Cyclic in-situ testing, crack segmentation and crack volume fraction, *Composites Communications*, 21, Article 100384.
- [14] Chai Y., Wang Y., Yousaf Z., Vo N.T., Withers P.J. (2020), Damage evolution in braided composite tubes under torsion studied by in-situ X-ray computed tomography, *Composites Science and Technology*, 1881, Article 107976 (open access).

- [15] Wagner P., Schwarzhaupt S., May M. (2019), In-situ X-ray computed tomography of composites subjected to fatigue loading, *Materials Letters*, 2361, 128-130.
- [16] Watanabe T., Takeichi Y., Niwa Y., Hojo M., Kimura M. (2020), Nanoscale in situ observations of crack initiation and propagation in carbon fiber/epoxy composites using synchrotron radiation X-ray computed tomography, *Composites Science and Technology*, 1978, Article 108244 (open access).
- [17] Jo E., Lee S., Hong C., Ji W. (2020), In situ observation of interactive failure modes in a single-edge notched symmetric cross-ply laminate using synchrotron X-ray tomography, *Composites Part A: Applied Science and Manufacturing*, 128, Article 105661.
- [18] Hufenbach W., Böhm R., Gude M., Berthel M., Andrich M. (2012), A test device for damage characterisation of composites based on in situ computed tomography, *Composites Science and Technology*, 72, Issue 1223, 1361-1367.
- [19] *Tableau, N., Aboura, Z., Kbellil, K., Laurin, F., & Schneider, J. (2019). Multiaxial loading on a 3D woven carbon fiber reinforced plastic composite using tensile-torsion tests: Identification of the first damage envelope and associated damage mechanisms. Composite Structures. Volume 227*
- [20] *A.S.Chen, F.L.Matthews. (1993). A review of multiaxial/biaxial loading test for composite materials Composites. Volume 24, Pages 395-406.*
- [21] *A. Catherine Davy, Didier Marquis. (2003). A multiaxial failure criterion for a brittle orthotropic composite, Materials & Design, Volume 24, Issue 1, Pages 15-24*
- [22] *J. Navarro-Zafra, J.L. Curiel-Sosa, and M.C. Serna Moreno, "Mixed-mode damage into a CGRP cruciform subjected to biaxial loading", Composite Structures, vol. 133, pp. 1093-1100, 2015.*
- [23] *J.L.Y. Tan, V.S. Deshpande, and N.A. Fleck, "Failure mechanisms of a notched CFRP laminate under multi-axial loading", Composites Part A: Applied Science and Manufacturing, vol. 77, pp. 56-66, 2015.*
- [24] *Found MS.: Review of the multiaxial fatigue testing of fiber reinforced plastics January Multiaxial fatigue. ASTM STP 8531985. p. 381-95.*
- [25] *Chen AS, Matthews FL. A review of multiaxial/biaxial loading tests for composite materials. Composites 1993;24(5):395-406.*
- [26] *Cytec Engineering Materials, CYCOM® PR 520 RTM Resin System, 00012, 19 March 2012*